JOURNAL OF THERMOPHYSICS AND HEAT TRANSFER
Vol. 24, No. 4, October–December 2010

Thermal Performance of Cylindrical Heat Pipe Using Nanofluids

K. N. Shukla*
Gurgaon College of Engineering, Gurgaon 122 413, India
and
A. Brusly Solomon,† B. C. Pillai,‡ and Mohammed Ibrahim§
Karunya University, Coimbatore 641 114, India

DOI: 10.2514/1.48749

A cylindrical copper heat pipe with a 19.5 mm outer diameter and a 400.0 mm length was filled with three different working fluids and tested for different heat inputs in the range of 100–250 W. The working fluids tested were de-ionized water, silver–water colloid, and copper water. Experimental results showed that the wall temperature reduction obtained was 3–27°C. The efficiency of the heat pipe was enhanced by 14% as compared with the heat pipe filled with the base fluid. Furthermore, it was found that an increase in the metal fraction in copper–water nanofluids lead to enhancement in thermal efficiency of the heat pipe. Thermal conductivities of copper–water nanofluids were measured, showing a 30% enhancement with a 0.1 wt % of copper nanoparticles.

Nomenclature

A	=	cross-sectional area
a	=	thermal diffusivity
c_p	=	specific heat of cooling water
d	=	wick diameter
g	=	gravity
K	=	permeability of wick
L	=	length
$\dot{m}$	=	mass flow rate of cooling water
Q	=	heat transfer rate
q	=	heat flux
R	=	heat pipe radius
r	=	radial coordinate
r_{cr}	=	critical radius
T	=	temperature
t	=	time
ΔP	=	pressure drop
ΔT	=	temperature difference
δ	=	film thickness
ϵ	=	porosity of wick
λ	=	heat of vaporization
μ	=	viscosity
ρ	=	density
σ	=	surface tension
ϕ	=	volume fraction of nanoparticles

Subscripts

a	=	adiabatic
c	=	condenser
e	=	evaporator
eff	=	effective
h	=	hydraulic
i	=	inner
l	=	liquid
o	=	outer
sat	=	saturation
v	=	vapor
w	=	wire
w, l	=	wall
ω	=	wick

Presented as Paper 2010-1364 at the 48th AIAA Aerospace Sciences Meeting including the New Horizons Forum and Aerospace Exposition, Orlando, FL, 4–7 January 2010; received 1 January 2010; revision received 29 July 2010; accepted for publication 30 July 2010.

*Director. Associate Fellow AIAA.
†Scientific Officer, Center for Research in Thermal Management.
‡Dean, Research; Director, Center for Biomass Energy.
§Research Associate, Center for Renewable Energy.

I. Introduction

IT IS well known that the thermal properties of heating or cooling fluids play a major role in the development of energy-efficient heat transfer equipment. However, conventional heat transfer fluids (such as ammonia, water, methanol, and glycol) and engine oils have, in general, poorer heat transfer properties than most solids [1,2]. There have been some attempts to improve the heat transport capability of the working fluids by adding some ultrafine metal particles to the base fluids to produce nanofluids. Wang et al. [3] measured the thermal conductivities of nanoparticles in fluid mixtures. Xuan and Qiang [4] presented a procedure of preparing nanoparticle suspension. They measured thermal conductivities of Cu nanoparticle suspensions in transformer oil and water and compared the enhancement in their thermal conductivities by developing a theoretical model. It was also observed that the thermal conductivity of nanofluids depends on the suspension and stability of the nanofluids and is improved by adding laurite salt. Liu et al. [5] presented the enhancement of the thermal conductivity of water in the presence of copper using the method of chemical reduction. They observed that the thermal conductivity was enhanced by 23.8% for Cu nanoparticles at a volume fraction of 0.001. Kim and Peterson [6] studied the effect of the morphology of carbon nanotubes on the enhancement of thermal conductivity of aqueous fluids. Wright et al. [7] reported the enhancement of thermal conductivity of heat transfer nanofluids containing a Ni-coated single-wall carbon nanotube by an applied magnetic field. At the first scientific conference centered on the theme "Nanofluids: Fundamentals and Applications" (16–20 September 2007, Copper Mountain, Colorado), it was decided to launch an International Nanofluid Property Benchmark Exercise (INPBE) to resolve the inconsistencies in the database and help advance research on nanofluid properties. Based on the reports on INPBE, Buongiorno et al. [8] presented the benchmark data of the thermal conductivity for the various nanofluids. Xu et al. [9] performed an experimental study of convective heat transfer of self-assembled ethanol-in-polyalphaolefin nanoemulsion fluids and

studied the thermophysical properties, including thermal conductivity and viscosity, and their dependence on temperature. The thermal conductivity enhancement in these fluids is found to be moderate but increases rapidly with increasing temperature in the measured temperature range of 35–75°C. A very remarkable increase in the convective heat transfer coefficient, by a factor of 2.2, occurs in the nanoemulsion fluids due to the explosive vaporization of the ethanol nanodroplets at the superheat limit (i.e., spindle states, about 122°C higher than the atmospheric boiling point for ethanol). Such an explosive liquid–vapor phase transition might augment the fluid heat transfer through the heat of vaporization (which intuitively raises the base fluid specific heat capacity) and the fluid mixing induced by the sound waves. The development of such phase changeable nanoemulsion fluids would open a new direction for thermal fluid studies.

The heat transfer phenomenon of the nanofluid was analyzed in various studies. For example, Zhou [10] experimentally investigated the heat transfer characteristics of copper nanofluids subjected to acoustic cavitations. They prepared an acetone-based copper nanofluid suspension and observed that the single-phase heat transfer was enhanced due to the addition of a small amount of nanoparticles while boiling heat transfer was reduced. Nguyen et al. [11] presented an experimental heat transfer enhancement using an alumina–water mixture for cooling a microprocessor and other electronic components. They found that the heat transfer coefficient was enhanced up to 40%, as compared with the base fluid for the volume concentration of 6.8%. He et al. [12] presented the flow behavior and the heat transfer regimes (both laminar and turbulent) for a vertical pipe. Convective heat transfer characteristics in the developing region of tube flow with constant heat flux using alumina–water nanofluids were studied by Anoop et al. [13]. They also studied the effect of particle size on heat transfer in a laminar region.

Nanofluids have been considered as the working fluid for heat pipes in electronic cooling applications. Tsai et al. [14] have examined the effect of structural characteristics of nanoparticles on the thermal performance of a heat pipe with nanofluids and observed that the thermal resistance of the heat pipes with nanofluid was lower than the distilled water. Similar thermal resistance reduction was observed in the experimental investigation of grooved heat pipes charged with nanofluids by Kang et al. [15]. Park and Ma [16] studied the effect of nanofluid on heat transport capability in a well-balanced oscillating heat pipe. They observed that the maximum resistance reduction of about 50% was observed for 10-nm-sized particles, and the reduction was 80% for the particle size of 35 nm when compared with de-ionized (DI)-water-filled heat pipes. Liu et al. [17] tested a flat heat pipe with CuO/water nanofluid. The experiment confirmed that the boiling heat transfer characteristics of the miniature flat heat pipe evaporator can evidently be strengthened by using water/CuO nanofluids. Also observed was that the heat transfer coefficient and critical heat flux increase with the increase of the concentration when the mass concentration is less than 1%. Naphon et al. [18] studied the effect of titanium nanofluids on heat pipe performance for different percentages of nanoparticles and at different tilt angles and fluid charges. They also showed that the heat pipe efficiency was 10.60% higher than that with the base fluid for a 0.1% volume concentration. In another study, Naphon et al. [19] presented an enhancement of heat pipe efficiency with refrigerant–nanoparticle mixtures. The refrigerant R11 was used as a base working fluid, and the size of the titanium/R11 nanofluid was 21 nm. They found that the efficiency of the heat pipe was enhanced 1.40 times higher than that with pure refrigerant for a 0.1% nanoparticle concentration. The performance of sintered heat pipe was studied by Kang et al. [20] using 10- and 35-nm-sized silver nanofluids. They concluded that the wall temperature was reduced by 0.56 to 0.65°C compared with DI-water-filled heat pipe.

The improvement in the thermal conductivities leads to improvement in the heat transfer characteristics of the working fluids. This paper presents a study on the improvements in the thermal properties of the nanofluids, which subsequently leads to the enhancement of heat transport capability of the heat pipes at the moderate heat inputs of 100 to 250 W.

II. Nanofluids Preparation and Characterization

A. Preparation

1. Silver–Water Nanofluids

All chemicals used in this investigation are regent grade materials. Silver nitrate was used as a silver ion source. Ascorbic acid was used to diffuse the silver ions to the surface of the silver seeds. Trisodium citrate, used as a reducing agent, also acted as a capping agent. Sodium borohydride was used for rapid reduction of silver ions in large numbers. Polyvinyl pyrrolidone was used to avoid the aggregation of the silver particles. The purity of these chemicals is given in Table 1.

Preparation of silver colloid was done by a two-step reaction. In the first step, a large number of silver seeds were prepared and, in the second step, the growth of the silver seed particles was obtained by imposing the silver ions on the surface of the silver seeds. In the first step, 10.0 ml of aqueous $AgNo_3$ [0.25 millimolar (mM)] and 10.0 ml of trisodium citrate (0.25 mM) are rinsed well with the 0.6 ml solution of sodium borohydride (0.01 M). The color of the solution immediately turns to yellow. The change of color confirms the silver seed present in the solution. In the second step, 10.0 ml of an aqueous solution of polyvinylpyrrolidone (1 wt %), seed solution (0.1 ml), trisodium citrate (0.3 ml, 25 mM), and ascorbic acid (0.05 ml, 0.1 M) are mixed with the silver nitrate ($AgNO_3$; 0.25 ml, 0.01 M), and this solution is maintained in the ambient environment for 2 h. In the second reaction, there are no particles generated, but the silver particles from the seed solution will be grown, because the silver ions were imposed on the wall surface of the seed particles by the ascorbic acid. The color of the solution will slowly turn green. From this change of color, we can identify the growth of silver particles. The size of the particles was measured using a scanning electron microscope (SEM). The detailed procedure for preparing silver colloids with different particle sizes and different morphologies was given in Ledwith et al. [21]. The SEM (JSM 6390 model) image shows the different sizes of silver particles present in the colloid (see Fig. 1).

2. Copper–Water Nanofluid

Copper nanoparticles of 99.5% purity were prepared using a laser evaporation process by Na-Bond Technologies. Copper–water nanofluid suspensions were prepared by ultrasonic cavitations using an ultrasonic processor (UP400S). DI water with 0.01 and 0.1 wt % of copper particles was kept under ultrasonic cavitations for about 30 min. Particles were dispersed by the production of fine bubbles in the sonotrode. The copper particles were dispersed completely after a few minutes, which can be seen by the change of the color. Particle size was viewed using SEM, and it was observed that the fluid contained the particle sizes of 80 to 130 nm (see Fig. 2 for image of the copper nanoparticles).

B. Viscosity of the Nanofluids

A Brookfield LVDR-II+ model viscometer was used to measure the viscosity of the nanofluids. The viscosity of the silver nanofluids was measured immediately (once) and after one month of preparation. It was observed that the viscosity of the nanofluids possesses time-dependent characteristics. Viscosity was also measured at different temperatures, which again showed temperature-dependent characteristics, a phenomenon by which liquid viscosity tends to decrease (or, alternatively, its fluidity tends to increase) as its temperature increases (see Fig. 3). The freshly prepared silver–water nanofluid exhibits almost Arrhenius characteristics, which change to

Table 1 Chemicals with different grades of the purity

Chemicals	Purity	Supplier
Silver nitrate ($AgNo_3$)	99.9	Merck Co.
Ascorbic acid ($C_6H_8O_6$)	99.7	Merck Co.
Trisodium citrate [$C_6H_5Na_3O_7 \cdot 2(H_2O)$]	99.0	Merck Co.
Sodium borohydride ($NaBH_4$)	$\geq$ 95.0	Merck Co.

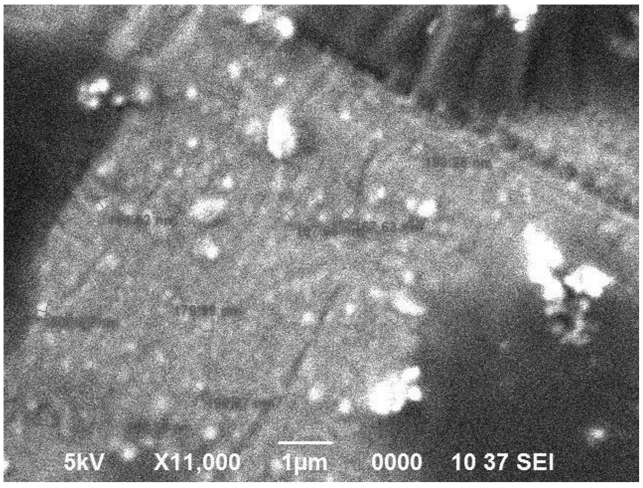

Fig. 1 SEM image of silver particles (SEI denotes secondary electron image).

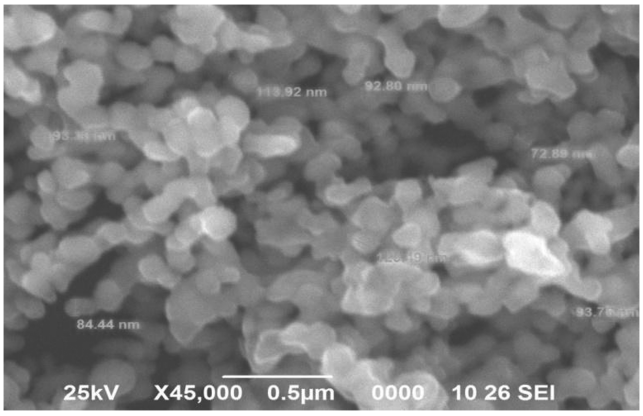

Fig. 2 SEM image of Cu nanoparticles.

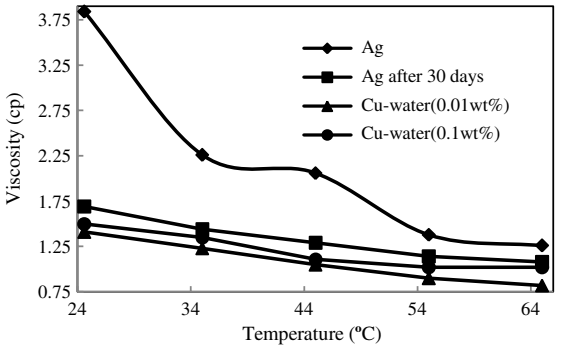

Fig. 3 Viscosities of nanofluids.

linear after 30 days. Similar behavior is seen for the copper–water nanofluids with weight percentages of 0.01 and 0.1, respectively. The main reason for the Arrhenius characteristics of the Ag colloid is due to the growth process of Ag particles. The complete growth of silver particles took 2 h at an ambient temperature, and this growth of the Ag particle varied with respect to the temperature [22].

C. Thermal Conductivity of Nanofluids

A basic experimental setup for measuring the thermal conductivity of the nanofluids was developed. A transient hot-wire method was used to measure the thermal conductivity. The principle of the transient hot-wire apparatus is that an infinitely long, vertical, line source of heat possessing zero heat capacity and infinite thermal conductivity is immersed in a sample fluid in thermodynamic equilibrium with the line source. At time $t = 0$, when a heat flux q per unit length is imposed, the energy is entirely conducted from the line source to the fluid. For the line source of radius r_w and a uniform initial temperature, the temperature rise of the wire and the thermal conductivity of the fluid will follow the following relationship:

$$\Delta T(r_o, t) = \frac{q}{4\pi k} \ell_n \left(\frac{4at}{r_w^2 c} \right) \tag{1}$$

Equation (1) presents the fundamental relation of the transient hot-wire technique. The slope of the line ΔT vs logarithmic t determines the thermal conductivity of the fluid. However, the line heat source assumption is not justified for nanofluid application. Vadasz [22] studied the heat conduction process in the nanofluids, and Eq. (1) can be modified by introducing the finite thickness of the line source as

$$k = \frac{q_0 r_0}{[T_w(t) - T_c]} [-r_w \ell_n(r_w) + f(t)] \tag{2}$$

The correction factor $f(t)$ is defined as

$$f(t) = \sum_{n=1}^{\infty} C_n \exp(-k_n^2 t) \tag{3}$$

The eigenvalues k_n are the roots of Eq. (4):

$$J_0(k_n) Y_1(k_n r_w) - Y_0(k_n) J_1(k_n r_w) = 0 \tag{4}$$

The first three roots of the Eq. (4) are determined as 2.415, 5.535, 8.6537, and 11.81001 for $r_w = 0.00019$ m.

The coefficient C_n of Eq. (3) is defined as

$$C_n = \frac{\pi^2 r_w J_1^2(k_n r_w)[Y_0(k_n) J_0(k_n r_w - J_0(k_n) Y_0(k_n r_w)]^2}{2[J_0^2(k_n r_w) - J_1^2(k_n r_w)]} \tag{5}$$

where $J_0(k_n r)$ and $Y_0(k_n r)$ are the zeroth-order Bessel functions of the first and second kind, and $J_1(k_n r_w)$ and $Y_1(k_n r_w)$ are the first-order Bessel functions of the first and second kind, respectively. The series in Eq. (3) is highly convergent, and we require only a few terms for calculation to a reasonable degree of accuracy. In the transient thermal conductivity measurement apparatus fabricated for the present work, an epoxy-coated nickel–chromium wire with a 0.07 m length was used, with a wire radius of 0.00019 m. The nickel–chromium was used as a line source of heat. A thermocouple was placed very close to the heat source to measure the fluid temperature at different times. This heat source was immersed in the cell of a 16-mm-diam tube that contained sample nanofluids. Before measuring the thermal conductivity of the nanofluids, the hot-wire apparatus was calibrated by measuring a sample liquid with known thermal conductivity. The thermal conductivity of the copper–water nanofluid was determined for different weight percentages using the transient hot-wire method and applying Eq. (2). The average particle size of the copper particle was 80 nm. Figure 4 reveals that

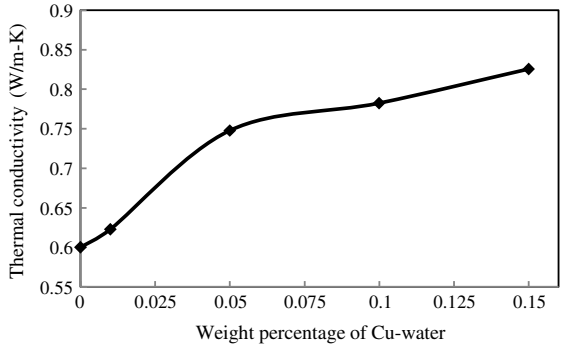

Fig. 4 Thermal conductivity of nanofluids.

the thermal conductivity of the nanofluids increases with the increase in the weight percentage of the copper nanoparticles. The thermal conductivity is enhanced by 3.79% for 0.01 wt % of copper particle and 30% for 0.1 wt % of copper particle. Similar thermal conductivity enhancement was observed in [3], while the copper oxide particle dispersed in water and ethylene glycol. They also found that the effective thermal conductivity of ethylene glycol increases 26% when approximately 5 vol % of alumina powders are added, and it increases 40% when approximately 8 vol % of alumina powders are added.

D. Surface Tension

The surface tension of nanofluids at different temperature is measured using a SITA DynoTester made by SITA Messtechnik, GmbH. The measuring range of the DynoTester is 15–100 mN/m, with a maximum error of 1%, which is given by the manufacturer. The measured surface tension profiles are presented in Fig. 5. There is no considerable variation in surface tension when metal particles are added with base fluids.

III. Experimental Setup and Testing for Heat Pipe Performance

Figure 6 presents the heat pipe setup and a schematic of the thermocouples mounted there. A copper tube 400 mm long with a 19.5 mm outer diameter was taken, and both ends were sealed with end caps. One end cap carried the filling tube for charging the working fluid. A 100-mesh copper screen was fixed on the inner tube, which was supported by a spring setup. This metal tube was also maintained at a vacuum condition up to 8 h, and a working fluid was injected through a capillary tube by adjusting the valve. The capillary tube was then crimped and sealed. The evaporator and adiabatic and condenser sections are of the lengths 100, 200, and 100 mm, respectively. The isothermal boundary condition was ensured in the adiabatic section by glass wool insulation. The heat transfer capacity was improved by providing 14 numbers of flat fins, each with a 0.5 mm thickness, mounted on the condenser section by brazing.

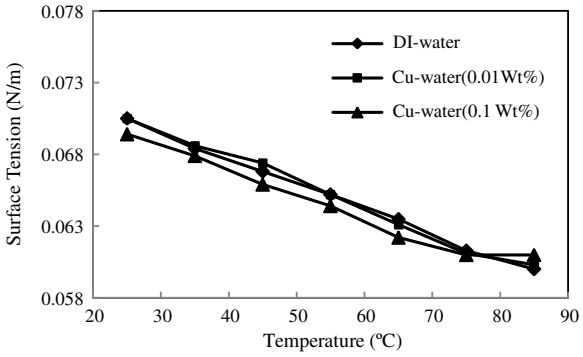

Fig. 5 Surface tension of nanofluids.

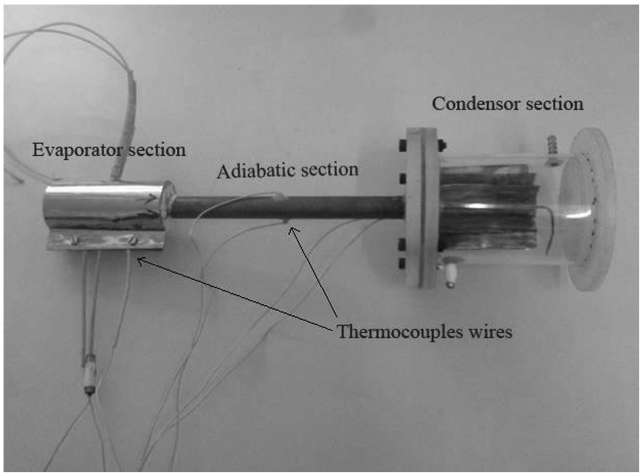

Fig. 6 Heat pipe setup.

The experimental setup consists of a resistance heater (maximum power output of 1000 W), a watt meter, and a variable transformer to provide supply to the heaters. The data acquisition consisting of a data logger (Yyokogawa) and a PC system recorded the thermocouple readings at different positions of heat pipe. The thermocouples of the K type in 10 numbers were used to measure the temperature response at the different heat pipe sections. In each section, there were two thermocouples to measure the temperatures. The inlet and outlet temperatures of the cooling water were measured using two T-type thermocouples. The flow rate of the cooling water was measured when the heat pipe operated steadily. The heat pipe with base fluids and nanofluids was tested for heat input varying from 100 to 250 W.

After the complete insulation of the heater and the adiabatic section, the power supply to the resistance heater unit was turned on. The heat input was varied using the variable transformer from 100 to 250 W. The temperature at different positions of the heat pipe was monitored by the data acquisition unit and so were the inlet and outlet temperatures of the cooling water (see Fig. 7). The mass flow rate of the condensate water was measured when the heat pipe operated steadily. The errors in the measuring instruments are presented in Table 2.

IV. Performance of Heat Pipe with Nanofluids

To study the thermal performance of the heat pipe, the heat transfer rate from the condenser was evaluated as

$$Q_{\text{exp}} = \dot{m} c_p (T_{w,o} - T_{w,i}) \tag{6}$$

where $\dot{m}$ represents the mass flow rate of cooling water, and $T_{w,i}$ and $T_{w,o}$ are the inlet and outlet temperatures of the cooling water. As the heat flux through the heat pipe wall is balanced by the heat flux in the liquid film q, we get

$$\Delta T = T_{\text{sat}} - T_{w,l} = q\left[\frac{\delta}{k_l} + \frac{R_i}{K_w}\ln\left(\frac{R_0}{R_i}\right)\right] \tag{7}$$

The film thickness $\delta = k/h$ is obtained from the heat transfer correlation reported by Cengel [23]:

$$h = 0.555\left\{\frac{g\rho_l(\rho_l - \rho_v)k_l^3}{\mu_l(T_{\text{sat}} - T_{w,l})}\left[\lambda + \frac{3}{8}C_{pl}(T_{\text{sat}} - T_{w,l})\right]\right\}^{1/4} \tag{8}$$

The iterative computation of ΔT vs heat input in the condenser is shown in Fig. 8. There is a linear variation of the temperature with respect to the heat input for the nanofluids. The nanofluid of copper–water performs better than the nanofluid of DI water.

The wall temperature of the heat pipe at different heat inputs is presented in Figs. 9a–9d. When compared with heat pipes filled with

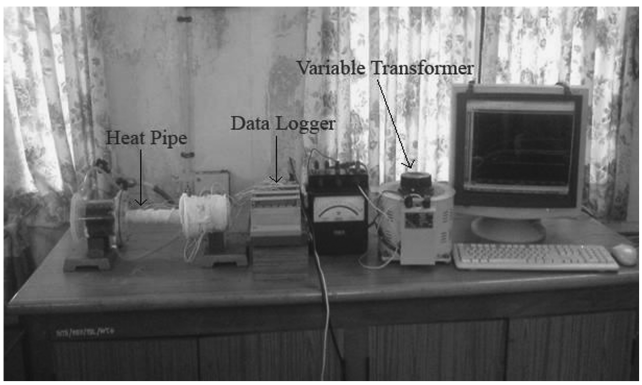

Fig. 7 Heat pipe experimental scheme.

Table 2 Error specification

Instruments	Errors
Thermocouple K type, data logger	±0.1°C
Watt meter, W	±1.5%
Flow measurement, kg/s	±2%

the base fluid, the nanofluid-filled heat pipes show a reduction in the wall temperature. The wall temperature reduces when the percentage of the copper weight increases. From the experimental result, it is observed that the average evaporator wall temperature is reduced in the range of 3 to 23°C, the average adiabatic wall temperature is reduced in the range of 4 to 27°C, and the average condenser wall temperature is reduced in the range of 3 to 6°C. This wall temperature reduction leads to reduction in resistance or increase in the thermal conductivity of the heat pipes. The temperature is uniformly maintained in the adiabatic region of the heat pipe in all the cases while the diffusion is predominant in the liquid-vapor region of the condenser.

The main reason for temperature reduction is the presence of a large number of bubble nucleation sites created in the evaporator section. This nucleation site creates a high thermal resistance that prevents the transfer of heat from solid surface to liquid. The suspended nanoparticle tends to bombard the vapor bubble during the bubble formation. Therefore, it is expected that the nucleation size of the vapor bubble is much smaller for fluid with suspended nanoparticles than without them [14]. To analyze the nanoparticle deposition on the wick surface, the wick sample from the evaporator section was obtained by cutting the heat pipe after the experiments. The surface condition of the wick surface was then observed by SEM (made by JEOL, Ltd.). The observed SEM image (see Fig. 10) shows the nanoparticle deposition on the wick surface and the forming of a microporous structure/layer on the evaporator wall. The presence of the microporous layer can help delay the critical heat flux in two ways. First, its increased wettability promotes rewetting upon bubble departure. Second, the layer may assist in dissipating the hot spot by enhancing radial conduction on the surface. Of course, the magnitude of the radial conduction is small in the thin layer of the microporous structure. This reduces the wall temperature of the heat pipe.

V. Capillary Limit of the Heat Pipe

The maximum heat transport capability of the heat pipes depends upon its capillary limit. This can be calculated by neglecting the axial hydrostatic pressure drop, the initial pressure gradient in the evaporator, and the pressure gradient across the phase transitions. The capillary limit of the heat pipe can be written as

$$\frac{2\sigma\cos\theta}{r_c} = \frac{16\mu_v L_{\text{eff}} Q}{2r_{h,v}^2 A_v \rho_v \lambda_v} + \frac{\mu_l L_{\text{eff}} Q}{K A_\omega \rho_l \lambda_l} + \rho_l g d_v \tag{9}$$

and by simplifying for the capillary limit Q, we get

$$Q = \left(\frac{2\sigma\cos\theta}{r_c} - \rho_l g d_v\right)\left[\frac{16\mu_v L_{\text{eff}}}{2r_{h,v}^2 A_v \rho_v \lambda_v} + \frac{\mu_l L_{\text{eff}}}{K A_\omega \rho_l \lambda_l}\right]^{-1} \tag{10}$$

The wick permeability K can be calculated from the next equation:

$$K = \frac{d_\omega^2 \epsilon^3}{122(1-\epsilon)^2} \tag{11}$$

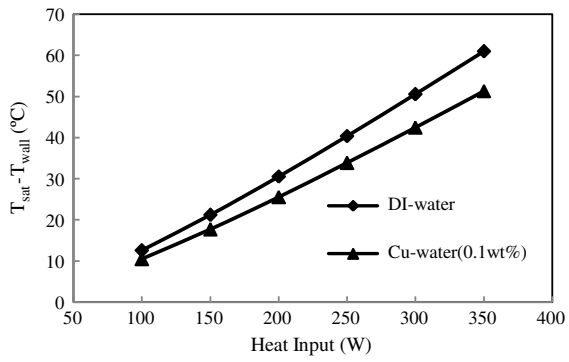

Fig. 8 Heat transfer rate vs temperature difference between vapor and wall.

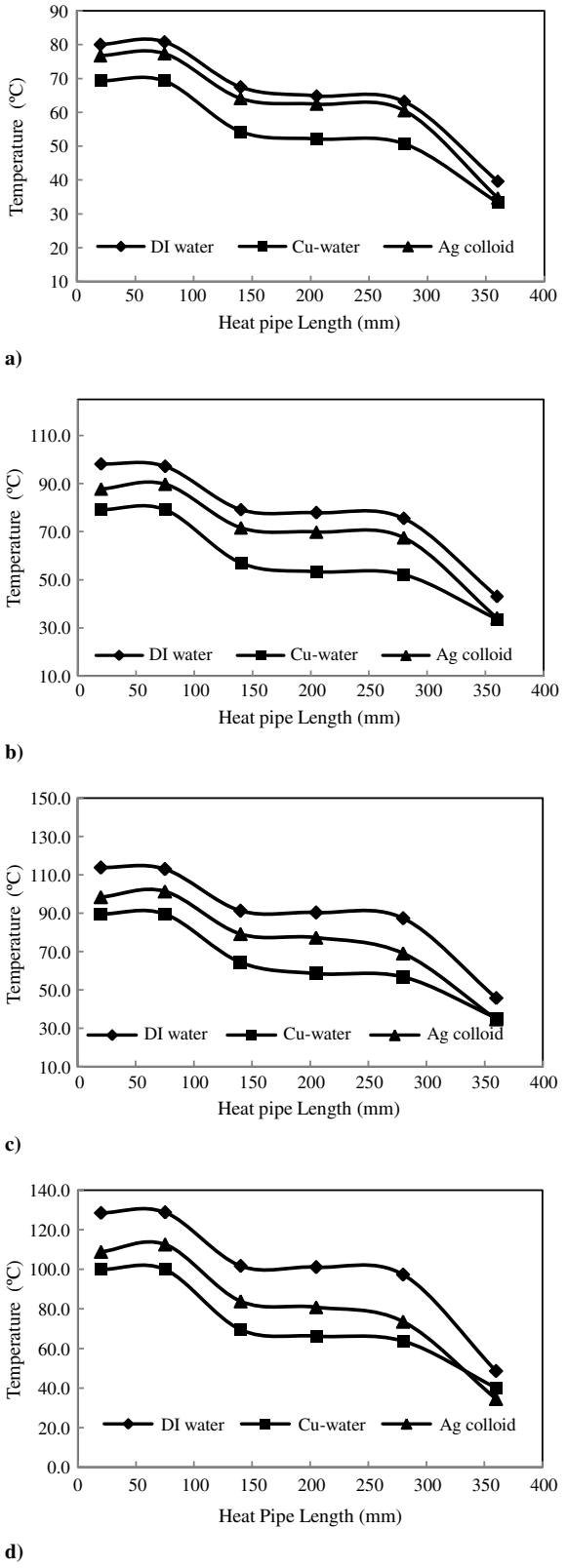

Fig. 9 Thermal performance of the heat pipe: a) 100, b) 150, c) 200, and d) 250 W.

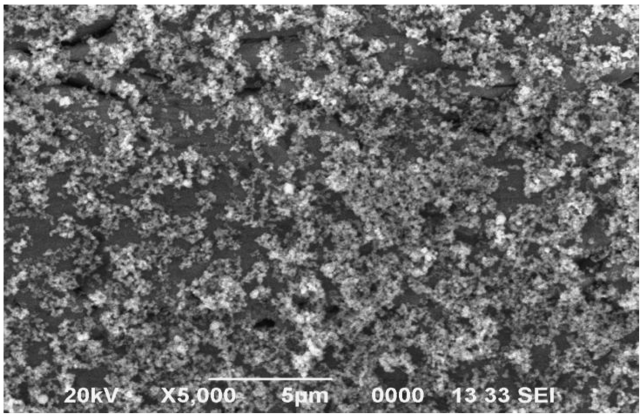

Fig. 10 SEM view of particle deposition.

The porosity of the wick is defined as

$$\epsilon = 1 - \frac{1.05\pi N d_w}{4} \tag{12}$$

where N denotes the number of wires per inch in a sintered wire mesh. The capillary limit of the heat pipe was calculated for the different nanofluids. Figure 11 shows the heat transport limitation of the heat pipe with different nanofluids. There is an enhancement in the heat transport capability with the application of the nanofluids, since the viscosity of the nanofluids tends to decrease with the increase of the temperature. The copper–water nanofluid performs better than the DI water nanofluid.

VI. Heat Pipe Efficiency with Different Nanofluids

The heat transfer through the heat pipe Q_{out} was determined by applying an energy balance at the condenser water jacket given by

$$Q_{\text{out}} = Q_{\text{exp}} = \dot{m} c_p (T_{w,o} - T_{w,i}) \tag{13}$$

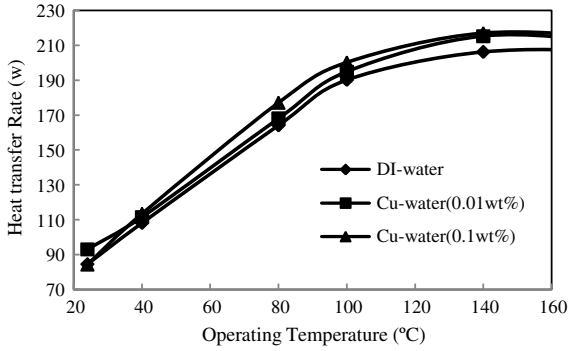

Fig. 11 Capillary limit of the heat pipe charged with the nanofluids.

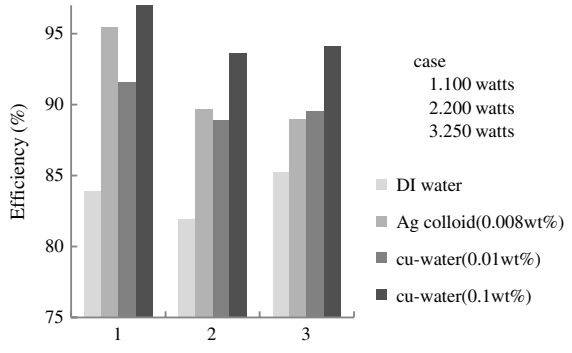

Fig. 12 Thermal efficiency of the heat pipe.

Table 3 RMSE at different heat inputs

Heat input, W	RMSE	Working fluids	RMSE
100	0.0615	Water	0.0162
200	0.0748	Ag	0.0311
250	0.0352	Cu (0.01)	0.0125
		Cu (0.1)	0.0224

Heat applied at the evaporator section of the heat pipe is measured using watt meters, and the efficiency of the heat pipe is calculated as

$$\eta = \frac{Q_{\text{out}}}{Q_{\text{in}}} \times 100\% \tag{14}$$

Figure 12 shows an improvement in the thermal efficiency of the heat pipe after the use of the nanofluids. The efficiency also improves by increasing the weight of the copper in a copper–water nanofluid. At 100 W of power, the silver colloid and copper–water nanofluids have almost the same efficiency, while the copper–water performs better at a higher power input of 250 W. The efficiency is also increased by 10–14% with the copper nanofluid-filled heat pipe as compared with the base-fluid-filled heat pipe. There is also a 5% increase in the efficiency of the heat pipe charged with the copper nanofluid when the weight percentage of the copper is increased from 0.01 to 0.1. For the silver nanofluid with the weight percentage of 0.008, the efficiency was increased by 3–7%.

All experiments have random errors, which occur inevitably during measurements. These errors may be analyzed with the calculation of the root-mean-square of errors (RMSE), defined as

$$\text{RMSE} = \sqrt{\frac{1}{n}\left[\sum_{j=1}^{n}\left(\frac{Q_{j-}Q_{j,\text{exp}}}{Q_{j,\text{exp}}}\right)^2\right]} \tag{15}$$

where n is the size of the sample. Table 3 presents the RMSE values for different heat inputs and working fluids. The results are within a reasonable degree of accuracy.

VII. Conclusions

Heat pipes charged with silver–colloid and copper–water nanofluids were fabricated. Nanofluids with different weight percentages were prepared and tested. As the volume percentage of the copper in the nanofluid increases, the efficiency of the heat pipe also increases, which results in the increase in the heat transfer capability of the heat pipe. At the copper weight percentage of 0.1, the maximum efficiency variation of 14% was obtained. In a similar way for the silver weight percentage of 0.008 in a silver nanofluid, the efficiency increases up to 8% compared with the one filled with pure water. For copper nanofluid, the heat transport limit of the heat pipe was improved up to 10 W. Furthermore, the nanoparticles present in the nanofluid sit on nucleation sites; they can create more new active nucleation sites by splitting a single nucleation site into multiple ones and enhancing the boiling heat transfer. Thus, we obtain a low temperature profile.

Acknowledgments

The authors wish to thank the anonymous reviewers and Zhuomin Zhang for their helpful comments in the revision of the manuscript.

References

[1] Shukla, K. N., "Thermo Fluid Dynamics of Loop Heat Pipe Operation," *International Communications in Heat and Mass Transfer*, Vol. 35, No. 8, 2008, pp. 916–920. doi:10.1016/j.icheatmasstransfer.2008.04.020

[2] Shukla, K. N., "Heat Transfer Limitation of a Micro Heat Pipe," *Journal of Electronic Packaging*, Vol. 3, No. 2, 2009, Paper 024502. doi:10.1115/1.3103970

[3] Wang, X., Xu, X., and Choi, S. U. S., "Thermal Conductivity of Nano-Particle Fluid Mixture," *Journal of Thermophysics and Heat Transfer*,

Vol. 13, No. 4, 1999, pp. 474–480.
doi:10.2514/2.6486

[4] Xuan, Y., and Qiang, L., "Heat Transfer Enhancement of Nanofluids," *International Journal of Heat and Fluid Flow*, Vol. 21, No. 1, 2000, pp. 58–64.
doi:10.1016/S0142-727X(99)00067-3

[5] Liu, M- S., Lin, C- C., Tsai, C. Y., and Wang, C- C., "Enhancement of Thermal Conductivity with Cu Nanofluids Using Chemical Reduction Methods," *International Journal of Heat and Mass Transfer*, Vol. 49, Nos. 17–18, 2006, pp. 3028–3033.
doi:10.1016/j.ijheatmasstransfer.2006.02.012

[6] Kim, B. H., and Peterson, G. P., "Effect of Morphology of Carbon Nanotubes on Thermal Conductivity Enhancement of Aqueous Fluids," *Journal of Thermophysics and Heat Transfer*, Vol. 21, No. 3, 2007, pp. 451–459.
doi:10.2514/1.18341

[7] Wright, B., Thomas, D., Hong, H., Groven, L., Puszynski, J., Duke, E., Ye, X., and Jin, S., "Magnetic Field Enhanced Thermal Conductivity in Heat Transfer Nanofluids Containing Ni Coated Single Wall Carbon Nanotubes," *Applied Physics Letters*, Vol. 91, 2007, Paper 173116.
doi:10.1063/1.2801507

[8] Buongiorno, J., Venerus, D. C., Prabhat, N., McKrell, T., Jessica, T. J., and Rebecca, C. R., "A Benchmark Study on the Thermal Conductivity of Nanofluids," *Journal of Applied Physics*, Vol. 106, No. 9, 2009, Paper 094312.
doi:10.1063/1.3245330

[9] Xu, J. J., Wu, C. W., and Yang, B., "Thermal and Phase-Change Characteristics of Self-Assembled Ethanol/Polyalphaolefin Nanoemulsion Fluids," *Journal of Thermophysics and Heat Transfer*, Vol. 24, No. 1, 2010, pp. 208–211.
doi:10.2514/1.43752

[10] Zhou, D. W., "Heat Transfer Enhancement of Copper Nanofluid with Acoustic Cavitations," *International Journal of Heat and Mass Transfer*, Vol. 47, Nos. 14–16, 2004, pp. 3109–3117.
doi:10.1016/j.ijheatmasstransfer.2004.02.018

[11] Nguyen, C. T., Roya, G., Gauthier, C., and Galanis, N., "Heat Transfer Enhancement Using Al_2O_3–Water Nanofluid for an Electronic Liquid Cooling System," *Applied Thermal Engineering*, Vol. 27, Nos. 8–9, 2007, pp. 1501–1506.
doi:10.1016/j.applthermaleng.2006.09.028

[12] He, Y., Jin, Y., Chen, H., Ding, Y., Cang, D., and Lu, H., "Heat Transfer and Flow Behavior of Aqueous Suspensions of TiO_2 Nanoparticles (Nanofluids) Flowing Upward Through a Vertical Pipe," *International Journal of Heat and Mass Transfer*, Vol. 50, No. 11, 2007, pp. 2272–2281.
doi:10.1016/j.ijheatmasstransfer.2006.10.024

[13] Anoop, K. B., Sundararajan, T., and Das, S. K., "Effect of Particle Size on the Convective Heat Transfer in Nanofluid in the Developing Region," *International Journal of Heat and Mass Transfer*, Vol. 52, Nos. 9–10, 2009, pp. 2189–2195.
doi:10.1016/j.ijheatmasstransfer.2007.11.063

[14] Tsai, C. Y., Chien, H. T., Ding, P. P., Chan, B., Luh, T. Y., and Chen, P. H., "Effect of Structural Character of Gold Nanoparticles in Nanofluid on Heat Pipe Thermal Performance," *Materials Letters*, Vol. 58, No. 9, 2004, pp. 1461–1465.
doi:10.1016/j.matlet.2003.10.009

[15] Kang, S. W., Wei, W. C., Tsai, S. H., and Yang, S. Y., "Experimental Investigation of Silver Nanofluid on Heat Pipe Thermal Performance," *Applied Thermal Engineering*, Vol. 26, Nos. 17–18, 2006, pp. 2377–2382.
doi:10.1016/j.applthermaleng.2006.02.020

[16] Park, K., and Ma, H. B., "Nano Fluid Effect on Heat Transport Capability in a Well-Balanced Oscillating Heat Pipe," *Journal of Thermophysics and Heat Transfer*, Vol. 21, No. 2, 2007, pp. 443–445.
doi:10.2514/1.22409

[17] Liu, Z- H., Xiong, J. G., and Bao, R., "Boiling Heat Transfer Characteristics of Nanofluids in a Flat Heat Pipe Evaporator with Micro-Grooved Heating Surface," *International Journal of Multiphase Flow*, Vol. 33, No. 12, 2007, pp. 1284–1295.
doi:10.1016/j.ijmultiphaseflow.2007.06.009

[18] Naphon, P., Assadamongkol, P., and Borirak, T., "Experimental Investigation of Titanium Nanofluids on the Heat Pipe Thermal Efficiency," *International Communications in Heat and Mass Transfer*, Vol. 35, No. 10, 2008, pp. 1316–1319.
doi:10.1016/j.icheatmasstransfer.2008.07.010

[19] Naphon, P., Thongkum, D., and Assadamongkol, P., "Heat Pipe Efficiency Enhancement with Refrigerant–Nanoparticle Mixtures," *Energy Conversion and Management*, Vol. 50, No. 3, 2009, pp. 772–776.
doi:10.1016/j.enconman.2008.09.045

[20] Kang, S- W., Wei, W- C., Tsai, S- H., and Huang, C- C., "Experimental Investigation of Nanofluids on Sintered Heat Pipe Thermal Performance," *Applied Thermal Engineering*, Vol. 29, Nos. 5–6, 2009, pp. 973–979.
doi:10.1016/j.applthermaleng.2008.05.010

[21] Ledwith, D. M., Whelan, A. M., and Kelly, J. M., "A Rapid, Straight-Forward Method for Controlling the Morphology of Stable Silver Nanoparticles," *Journal of Materials Chemistry*, Vol. 17, No. 23, 2007, pp. 2459–2464.
doi:10.1039/b702141k

[22] Vadasz, P., "Heat Conduction in Nanofluid Suspensions," *Journal of Heat Transfer*, Vol. 128, No. 5, 2006, pp. 465–476.
doi:10.1115/1.2175149

[23] Cengel, Y. A., "Boiling and Condensation," *Heat Transfer: A Practical Approach*, 2nd ed., McGraw–Hill, New Delhi, Delhi, India, 2003, pp. 515–560.